Supporting Information

Generalized analysis approach of the profile roughness of hierarchically grown polystyrene-iron oxide-silica core-shell particles by electron microscopy

Deniz Hülagü[*], *Charlie Tobias, Estela Climent, Ardian Gojani, Knut Rurack*[*], *Vasile-Dan Hodoroaba*

1. Results and Discussion

1.1. Selection of Threshold Algorithm

Numerous segmentation techniques have been reported in the literature.[1, 2] Since these techniques were highly purpose-dependent, no standard procedure has been identified for EM images. A typical thresholding technique starts by partitioning the histogram of an EM image into two classes where pixels with intensity values less than the threshold are classified as background and the others are set as foreground.

IsoData algorithm and Otsu's algorithm are two of the most well-known methods of thresholding-based segmentation.[3] IsoData is a simple, and probably the first, automatic iterative approach for determining a threshold value.[4] An initial threshold value is first guessed, which is mostly taken to be the average intensity value of the image, to segment the image into two categories. The mean values of the pixels in the two categories are calculated and then the new threshold value is determined as the average of these two values. The new threshold is updated iteratively until the threshold value remains unchanged which gives the optimal threshold value. Otsu's approach is based on a variance-based objective function, where the optimum threshold is selected to give the best separation of classes by maximizing the between-class variance.[5]

To understand the influence of thresholding-based segmentation algorithm on our results, a preliminary test has been performed. TSEM images of a single PS/Fe_3O_4/SiO_2 particle recorded at several accelerating voltages (EHT) between 2 and 15 kV were binarized with two different threshold algorithms by the Gwyddion (http://gwyddion.net/) and ImageJ software

(https://imagej.nih.gov/ij/) while the threshold was set to the same value. Each software is commonly used by the AFM community to analyze the images for various purposes. The proposed image analysis procedure was applied to the binarized images, and the root-mean squared profile roughness (RMS-R_Q) of the particle was calculated (**Figure S*1***). The results revealed that the average calculated RMS-R_Q value of all methods was 20±2.0 nm, which means that the overall discrepancy within the selected methods is maximum 10%. This means that no significant difference was observed between algorithms and software. Considering the inevitable bias, the obtained data were in good agreement. According to these results, it can be concluded that to select one of these methods to obtain binarized images was convenient. Due to the ease of use, it was decided to apply the automated threshold based on the IsoData algorithm with Gwyddion software.

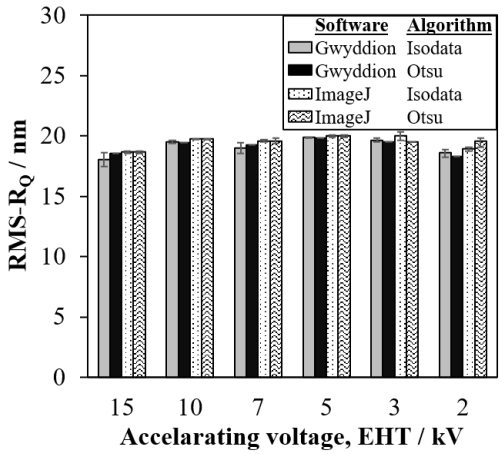

Figure S1 Result of application of different thresholding algorithms and image processing software by comparison of calculated profile roughness of a single PS/Fe_3O_4/SiO_2 particle from TSEM images recorded at various accelerating voltages (EHT) between 2 and 15 kV with different software and algorithms

2. Additional Particle Characterization

2.1. Scattering Properties in Flow Cytometry

Flow cytometry is an important method for single particle analysis. For the measurement, a particle suspension is brought into a flow-cell through a capillary. A stream of sheath fluid carries and aligns the particles via hydrodynamic focusing to pass a laser individually. The scattered light contains information about the size and the shape of the particles. The forward scattering (FSC) correlates with the volume of the particle, the side scattering (SSC) in turn depends on the structure and granularity of the particles. These scattering signals are characterized by a certain height (FSC-H, SSC-H), width (FSC-W, SSC-W) and area (FSC-A, SSC-A) recorded at the photomultiplier tube detector as the object passes the spot of the laser during its flow, transiting times usually being on the order of a few microseconds. For single-particle counting experiments of well-dispersed suspensions of spherical particles, plotting and analyzing the signal height, i.e., FSC-H and/or SSC-H, is usually sufficient to derive the relevant size and granularity information; absolute size information can however only be obtained by using appropriate reference particles. If particle sizes are more complex or anisotropic, a combination of FSC-H, FSC-W, SSC-H and SSC-W can further improve the analysis.[6]

Flow cytometric measurements were performed with a BD Accuri C6, recording FSC and SSC of the particles at 180° and 90°.[7] While the correlation of FSC and SSC data provides information on the dispersity, the SSC also reveals further information on the roughness. Flow cytometry measurements can thus provide complementary data to the roughness derived by the present image analysis approach. As shown in **Figure S2**, once coated with Fe_3O_4 and silica, the particles show increased scattering especially in the SSC-H channel, indicating a higher roughness of the surface in comparison to the PS core particles. However, it is evident from the dot plot of FSC-H and SSC-H that these particles are still highly monodisperse, as shown in **Figure S3.** It should be noted however that flow cytometry data can only reflect trends and

thorough calibration with adequate particles would be necessary to derive more quantitative information.

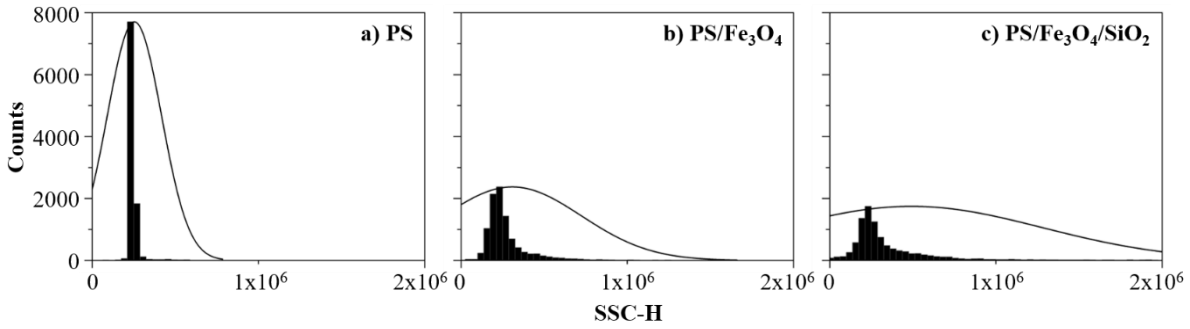

Figure S2 Histogram of the shape parameter (SSC-H) for (a) PS particles, (b) PS/Fe_3O_4 particles, and (c) $PS/Fe_3O_4/SiO_2$ particles; 10,000 particles counted for each measurement.

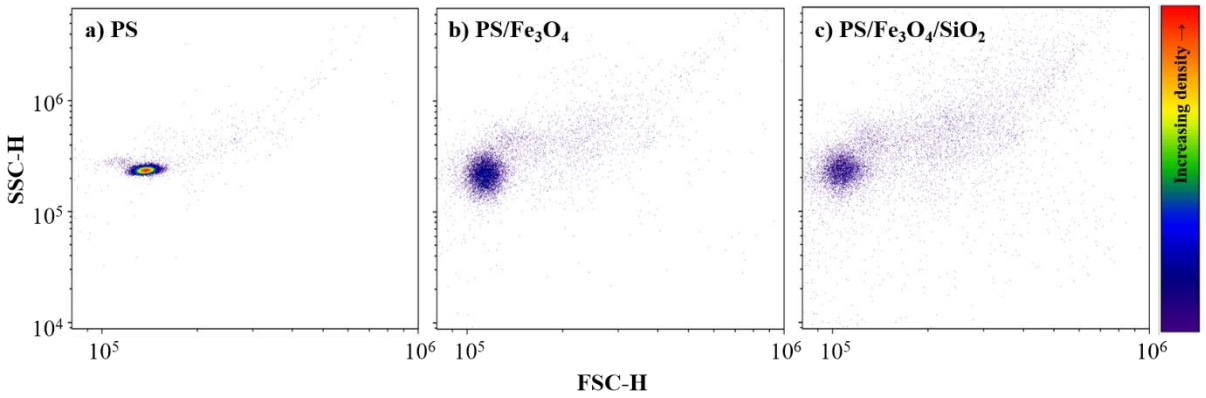

Figure S3 Density scattering plot with size (FSC-H) and shape (SSC-H) parameters for (a) PS particles, (b) PS/Fe_3O_4 particles and (c) $PS/Fe_3O_4/SiO_2$ particles.

3. Functionalization and Surface Charge

3.1. Ninhydrin Test of Aminated $PS/Fe_3O_4/SiO_2$ Particles

To assess the possibilities of further particle functionalization, amino groups (NH_2) were attached to the surface using 3-aminopropyltriethoxysilane (APTES). The amount of amino groups covalently grafted to the surface was determined with the ninhydrin test. In this test,

primary amines react with ninhydrin and produce the dye Ruhemann's Purple, which has an absorption maximum at 580 nm.[8] Functionalization of the shell can be easily accomplished via condensation of alkoxy silanes with the silanol groups of the outer silica shell. The ninhydrin test was performed with particles in which the silanol groups were previously activated under acidic conditions. After the activation and functionalization, the particles were still magnetic and had the same absorbance signal. The respective results are shown in **Table S1**, listing the absorbance and corresponding amounts of amino groups on the surface of the particles obtained from a calibration curve constructed from different amounts of pentyl amine being reacted with ninhydrin under identical conditions.

Table S1 Absorbance and amounts of amino groups on the surface of PS/Fe_3O_4/SiO_2 particles measured with ninhydrin test

Sample	Absorbance	[NH_2/nm^2]	Surface area [m^2 g^{-1}]
NH_2-PS/Fe_3O_4/SiO_2	0.022	7.3	7.6
NH_2-PS/SiO_2 [9]	0.015	6.6	8.1

The present particles display a slightly higher degree of functionalization than similar particles produced without the magnetic layer, i.e., ca. 7.3 compared to 6.6 molecules per nm^2.[9] However, as the size of an APTES molecule (length of ca. 0.45 nm) is small compared to R_Q values between ca. 2 and 20 nm, the fact that the four particle types with different surface roughness reported earlier by us and the present particles show very similar functionalization densities.

3.2. Zeta Potentials

To test the success of the different coating processes the Zeta potential was recorded for the various synthesis steps as shown in **Table S2**. The measurements were carried out with a

Zetasizer Nano-ZS from Malvern. The measurement is based on electrophoresis, the investigation of the motion of charged particles in an electric field, with the charge of the colloidal dispersion being directly related to its stability.[10] The particles showed the expected charge for each step. From the negatively charged pure PS, because of the carboxylate groups introduced via the initiator, and the positively charged iron oxide nanoparticles to the addition of the different layers. Adding the Fe_3O_4 nanoparticles to the PS core shifted the charge to a more positive value, which was reversed upon coating the second shell, consisting of silica.

Table S2 Results of Zeta potential measurements and the standard deviation of the measurements for the particles used in this work

Sample	Zeta potential [mV]	Standard deviation
PS	-49.2	1.0
Fe_3O_4	+6.7	0.6
PS/Fe_3O_4	-27.4	6.6
PS/Fe_3O_4/SiO_2	-44.0	3.2

4. Further Morphological Characterization

4.1. Characterization of Iron Oxide Nanoparticles

The aim of using polyvinylpyrrolidone (PVP) during the synthesis of the present particles was to prevent agglomeration of the iron oxide nanoparticles and to obtain a stable iron oxide nanoparticle dispersion. The dispersity of synthesized iron oxide nanoparticles was investigated by SEM and TEM. The samples were suspended in water and prepared on commercial copper TEM grids by spin-coating.

SEM images of the Fe_3O_4 nanoparticles, as shown in **Figure S*4***a, revealed that some of the particles are agglomerated, which is mainly caused by sample preparation. **Figure S*4***b shows a representative TEM image of the particles with a higher magnification than that of SEM.

The average size of the Fe_3O_4 nanoparticles was determined from TEM to d_{mean} = 7±1 nm. This size suggests that the iron oxide nanoparticles are superparamagnetic, as nanoparticles need to be sufficiently small (3-50 nm, depending on the material) to exhibit superparamagnetism.[11]

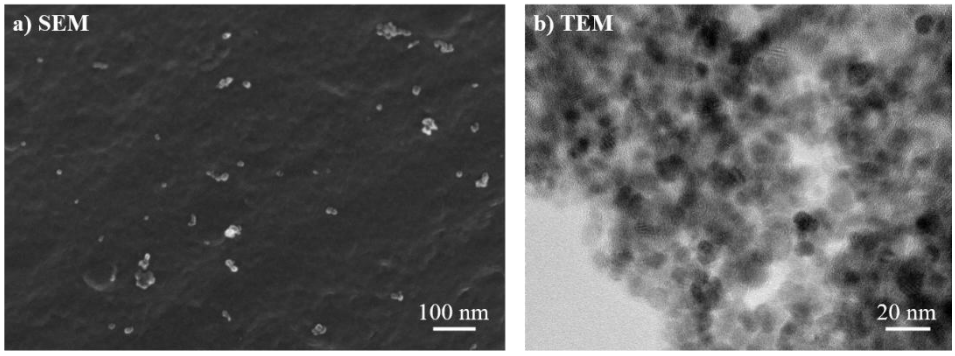

Figure S4 (a) SEM and (b) TEM images of Fe_3O_4 particles

4.2. Chemical Composition of PS/Fe_3O_4/SiO_2 Microparticles

The morphology of the PS/Fe_3O_4/SiO_2 core-shell-shell microparticles was analyzed by TEM as presented in **Figure S5**a. In the TEM image, the even distribution of Fe_3O_4 nanoparticles over the surface of the PS particle and the outer SiO_2 thin shell, covering the whole particle, are clearly visible.

Moreover, the chemical, i.e., elemental composition of the same particle has been investigated by Energy-Dispersive X-Ray Spectroscopy (EDS) and is presented in **Figure S5**b. A high carbon (C) peak intensity was detected, since carbon is the major constituent element of the particle core material itself, and silicon (Si) and iron (Fe) signals were also clearly detected, evidencing that the particle surface was covered with Fe_3O_4 and SiO_2.

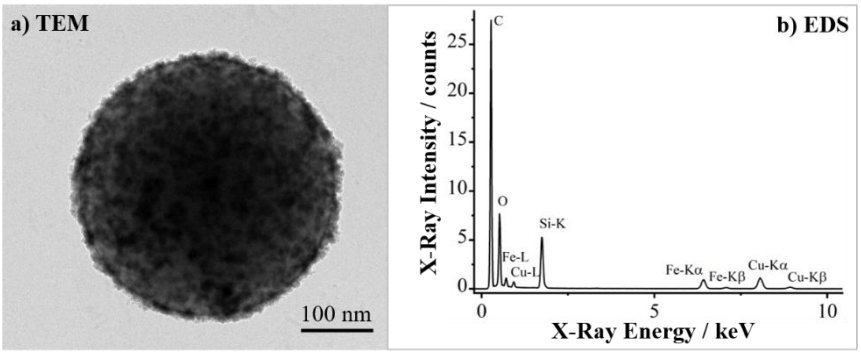

Figure S5 (a) TEM image of the PS/Fe_3O_4/SiO_2 microparticle and (b) EDS spectrum of the particle

Figure S6a, b present elemental mapping results of the PS/Fe_3O_4/SiO_2 microparticles by STEM and high-angle annular dark-field imaging (HAADF) and c and d present the close-ups of the same particle recorded by both techniques. The distinct SiO_2 shell on the PS core and the layer of Fe_3O_4 nanoparticles evenly spread over the whole particle surface can be discerned. The explanation why not a smooth silica shell significantly covers the PS/Fe_3O_4/SiO_2 particles is that the positions where the Fe_3O_4 nanoparticles were deposited before synthesizing the silica shell are visible, and the inorganic oxide shell incorporates the Fe_3O_4 particles, mediated by the PVP coating.

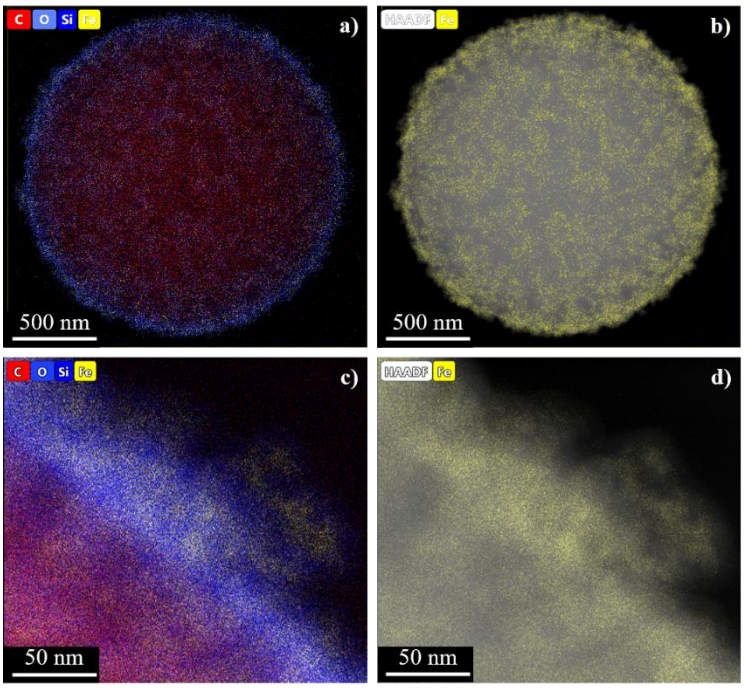

Figure S6 EDS mapping of elemental composition of a PS/Fe_3O_4/SiO_2 microparticle overlapped with (a) STEM and (b) HAADF images. (c) and (d) present close-ups of the same particle recorded by both techniques.

References

[1] C. Zheng, D. W. Sun, in *Computer Vision Technology for Food Quality Evaluation*, (Ed: D. W. Sun), Elsevier, San Diego, CA 2016, 45.
[2] K. S. Fu, J. K. Mui, *Pattern Recognit.* **1981**, *13*, 3.
[3] A. E. Vladár, V.-D. Hodoroaba, in *Characterization of Nanoparticles*, (Eds: V.-D. Hodoroaba, W. E. S. Unger, A. G. Shard), Elsevier, 2020, 7.
[4] T. W. Ridler, S. Calvard, *IEEE Trans. Syst. Man Cybern.* **1978**, *8*, 630.
[5] N. Otsu, *IEEE Trans. Syst. Man Cybern.* **1979**, *9*, 62.
[6] P. L. Mage, A. T. Csordas, T. Brown, D. Klinger, M. Eisenstein, S. Mitragotri, C. Hawker, H. T. Soh, *Nat. Mater.* **2019**, *18*, 82.
[7] J. A. Steinkamp, M. J. Fulwyler, J. R. Coulter, R. D. Hiebert, J. L. Horney, P. F. Mullaney, *Rev. Sci. Instrum.* **1973**, *44*, 1301.
[8] M. Friedman, L. David Williams, *Bioorg. Chem.* **1974**, *3*, 267.
[9] D. Sarma, K. Gawlitza, K. Rurack, *Langmuir* **2016**, *32*, 3717.
[10] R. W. O'Brien, L. R. White, *J. Chem. Soc., Faraday Trans.2* **1978**, *74*, 1607.
[11] V. Marghussian, in *Nano-Glass Ceramics*, (Ed: V. Marghussian), William Andrew Publishing, Oxford 2015, 181.